PROCEEDINGS OF SPIE

SPIEDigitalLibrary.org/conference-proceedings-of-spie

Addressing calibration of high-harmonic generation sources used for studying magnetism

Taylor Buckway, Aaron Redd, Devin Lewis, Eric Gullikson, Joshua Vawdrey, et al.

Taylor J. Buckway, Aaron Redd, Devin Lewis, Eric Gullikson, Joshua Vawdrey, Karine Chesnel, David Allred, Richard L. Sandberg, "Addressing calibration of high-harmonic generation sources used for studying magnetism," Proc. SPIE 12694, Advances in X-Ray/EUV Optics and Components XVIII, 1269404 (3 October 2023); doi: 10.1117/12.2692397

SPIE.

Event: SPIE Optical Engineering + Applications, 2023, San Diego, California, United States

Downloaded From: https://www.spiedigitallibrary.org/conference-proceedings-of-spie on 09 Oct 2023 Terms of Use: https://www.spiedigitallibrary.org/terms-of-use

Addressing Calibration of High Harmonic Generation Sources used for Studying Magnetism

Taylor J. Buckway[a], Aaron Redd[a], Devin Lewis[a], Eric Gullikson[b], Joshua Vawdrey[a], Karine Chesnel[a], David Allred[a], and Richard L. Sandberg[a]

[a]Department of Physics and Astronomy, Brigham Young University, N269 Eyring Science Center, Provo, USA
[b]Lawrence Berkeley National Laboratory, 1 Cyclotron Rd, Berkeley, USA

ABSTRACT

Tabletop extreme ultraviolet (EUV) sources based on high harmonic generation (HHG) have been used as a powerful tool for probing magnetism. Obtaining magnetic information via magneto-optical contrast often requires the energy of the light to be tuned to magnetic resonance energies of the magnetic element present in the material; therefore, it is essential to calibrate the HHG spectrum to well defined absorption energies of materials. We have designed and assembled a HHG based EUV source for studying transition metal magnetic materials at their resonant M-absorption edges (35-75 eV of photon energy). One material of interest is iron, for which the iron $M_{2,3}$ edge is 52.7 eV (23.5 nm wavelength) according to CXRO. We prepared and characterized a thin sample of iron for absorption spectroscopy and calibration of the absorption edge with beamline 6.3.2 at the Advance Light Source (ALS) in Lawrence Berkeley National Laboratory. This well characterized sample was capped with gold to prevent oxidation. From these measurements we extracted the absorption part of the index of refraction β spectrally and confirmed that the absorption edge of iron is 52.7 eV. With this information, we can better calibrate the HHG spectrum of our tabletop EUV source. Calibration of the HHG spectrum was achieved using model fitting the HHG spectrum using the grating equation and law of cosines while taking account into the results of the ALS data. We have determined that driving wavelength of the HHG process to be 773 nm. We also conclude that the chirp of the driving laser pulse can cause an energy shift to a HHG spectrum.

Keywords: Iron, High Harmonic Generation, HHG, Calibration, Magnetism, Magnetic materials, Binding energies, Spectroscopy

1. INTRODUCTION

High harmonic generation (HHG) is a powerful tabletop light source that generates highly coherent extreme ultraviolet (EUV) and soft x-ray radiation. HHG is described using the three step model developed by Corkham[1](see also[2–5]). The process involves focusing an intense ultrafast infrared laser beam onto a target gas. The intense electric fields cause extreme nonlinear up-conversion of the infrared radiation in the form of EUV and soft x-ray radiation. These sources are highly coherent and much more compact than their counterparts such as synchrotrons and free electron lasers. HHG sources are widely used for nanoscale imaging, spectroscopy, and studying ultrafast dynamics.[6–9] HHG sources are a powerful tool in studying the magnetism in magnetic material.[8–11]

Research in magnetic nanomaterials has led to technological advances in areas such as power generation, data storage, and medicine.[12] Ferromagnetic nanomaterials are often made up of tiny domains where a domains is a region of the material where all the atomic spins point in the same direction. One way to measure the amount of magnetization in the material is by using circular dichroism with polarized light and comparing absorption signal at opposite helicities fo the light polarization.[12–15] For example, X-ray magnetic circular dichroism (XMCD), when carried at the resonant edge, allows to extract information about the respective spin and orbital moment in the material. In addition, magnetic dichroism can be applied to scattering techniques, such as X-ray Resonant

Further author information:
Taylor J. Buckway: E-mail: taylorbuckway@gmail.com

Advances in X-Ray/EUV Optics and Components XVIII, edited by Hidekazu Mimura, Ali M. Khounsary, Christian Morawe, Proc. of SPIE Vol. 12694, 1269404
© 2023 SPIE · 0277-786X · doi: 10.1117/12.2692397

Downloaded From: https://www.spiedigitallibrary.org/conference-proceedings-of-spie on 09 Oct 2023
Terms of Use: https://www.spiedigitallibrary.org/terms-of-use

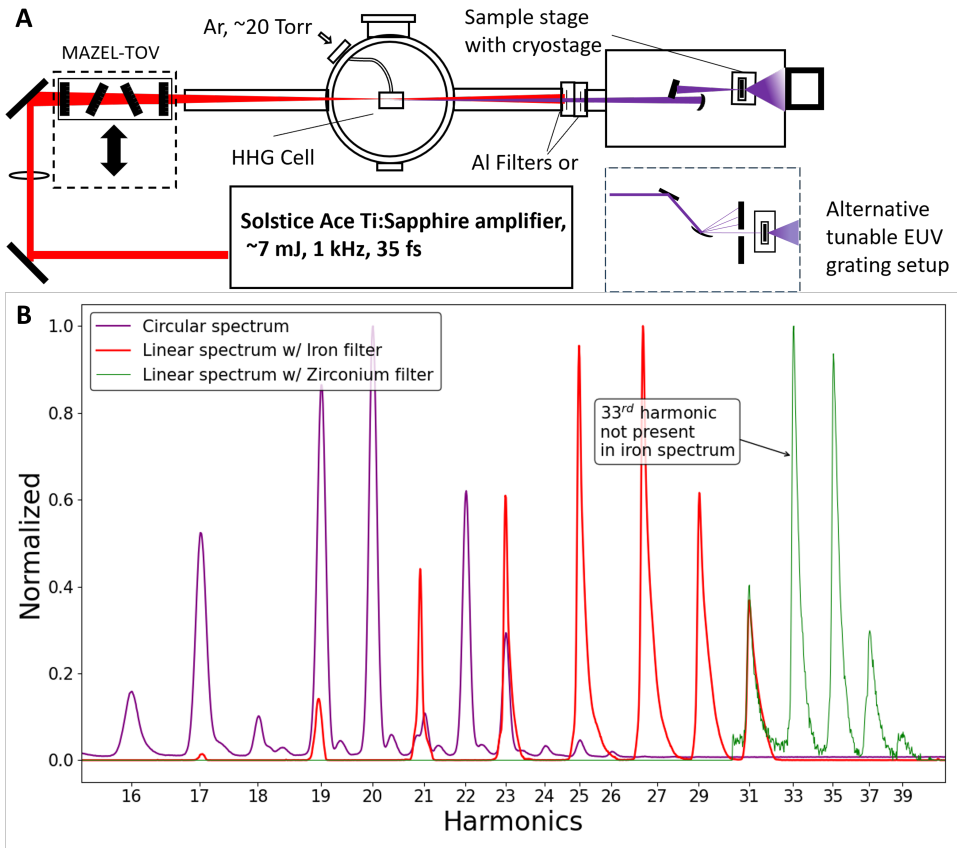


Figure 1. (A) Experimental setup of the HHG source at Brigham Young University. The high harmonics are generated in a finite argon gas cell. The driving beam is removed using aluminum filters and the harmonics are selected either by normal incidence mirrors or a grazing incidence spectrometer. Schematic taken from Buckway.[2] (B) Plot of the generated HHG spectrum: linear (red and green curves) and circular (purple curve) polarized spectra. Energy increases with harmonic order. The red and green linear spectra are the measured intensities with a 100 nm iron and 200 nm zirconium filters inserted, respectively. The zirconium is used instead of the iron filter to show additional harmonics beyond the 31st harmonic. The iron spectrum is used to identify the suppressed odd harmonics of the circular spectrum. The iron filter identifies which harmonic is near 52.7 eV.

Magnetic Scattering (XRMS) and imaging techniques, allowing to visualize the magnetic domains or magnetic correlations in the materials occuring at a scale larger than the X-ray wavelength. In all these techniques, the magneto-optical constrast is drastically enhanced when the x-ray energy is tuned to magnetic resonant edges. When transferring these x-ray techniques to the EUV range, it is therefore essential that the EUV source is calibrated correctly in order to tune photon energy to the proper magnetic resonances of the material. However, calibrating a high harmonic sprectrum accurately is challenging due to the dense nature of the harmonic spectrum, relatively broad spectrum, and in-vacuum requirement due the short wavelength.

We have built a HHG system at Brigham Young University for the purpose of imaging nanoscale magnetic domains at the resonant M-edges of transition metal materials (35-75 eV of photon energy).[2] Our HHG source is driven by a Spectra-Physics/MKS Solstice Ace Ti:Sapphire laser which generates 7mJ pulses that are 35 femtoseconds in duration with a central wavelength of 800 nm. The system is capable of generating both linearly and circularly polarized EUV light. The circularly polarized light is generated using the MAZEL-TOV apparatus.[16] A schematic of the HHG system is depicted in Fig. 1A. A flat silver mirror and a spherical grating were used as a spectrometer. The spherical grating has 1200 grooves per millimeter and its radius of curvature is two meters.

Fig. 1B shows the combined linear and circularly polarized spectra of the HHG source with the harmonics

Downloaded From: https://www.spiedigitallibrary.org/conference-proceedings-of-spie on 09 Oct 2023
Terms of Use: https://www.spiedigitallibrary.org/terms-of-use

identified. For circularly polarized harmonics, which require a combination of fundamental (800 nm) and second harmonic (400 nm) photons for generation, every third harmonic must be suppressed according to conservation of energy and angular momentum.[2,16–19] For linearly polarized spectra, only odd harmonics are allowed.[19–22] The odd harmonics of the linearly polarized spectrum are plotted with the circularly polarized spectrum to identify the suppressed odd harmonics of the circular spectrum. We used a 100 nm freestanding iron filter (Lebow Company) for calibrating the HHG spectrum. Fuggle et. al. reported iron $M_{2,3}$ edge resonance is 52.7 eV.[23–25] The suppressed odd harmonic constraint along with a thin metal filter can be used to identify the harmonic orders accurately in order to know which harmonic corresponds to a desired resonant absorption edge for magnetic transitions. In Fig. 1B, we identify the 21st suppressed odd harmonic. The linear spectrum is calibrated and the results are the red curve in Fig. 1B. The last harmonic of the iron spectrum is the 31st harmonic which would correspond to 48.4 eV for a driving wavelength of 800 nm. The 33rd harmonic, 51.2 eV, does not appear as it should when the iron filter is inserted. Our measured $M_{2,3}$ edge of iron from the HHG spectrum and those reported previously (CXRO Website tables) seem to contradict. The discrepancy we observed must be addressed before properly calibrating the HHG spectrum. Thus, we needed to either confirm the iron $M_{2,3}$ edge is at 52.7 eV or determine that the binding energy is actually lower as suggested in Fig. 1B.

2. EXPERIMENT

The measurement of the $M_{2,3}$ edge of iron was completed via absorption spectroscopy with beamline 6.3.2 at the ALS. This was then compared to the iron $M_{2,3}$ edge values on CXRO tables. Oxidation will cause the M-edge to blue shift (higher absorption energy) and so the sample must be protected.[9] We prepared two thin iron samples capped with gold using thermal evaporation. The iron and gold layers were deposited onto a silicon photodiode and a bare silicon wafer at the same time and without breaking vacuum between deposition. The iron sample on the photodiode was used for recording the transmission of photon energies from 35-75 eV. The iron on the silicon wafer was used for reflection at various angles using 159 eV (7.8 nm wavelength) for characterization of the sample. The samples and their characterization are shown in Fig. 2A-B, 3A. The thickness of the iron is 21 nm and it is capped by 10 nm of gold.

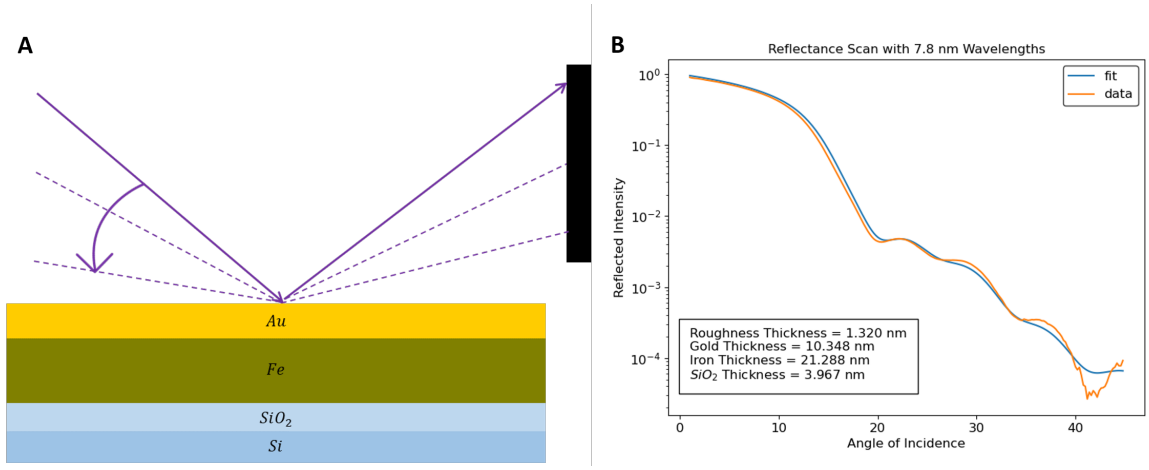


Figure 2. (A)Iron sample for reflection measurements. The sample is capped with gold and deposited on a silicon wafer for EUV reflection measurements to characterize the sample. (B) Reflectomety measurements from the multilayer stack, along with modeled reflectance for 10.3 nm of gold and 21.3 nm of iron. Measurements, with 159eV photon energy, were taken at beamline 6.3.2 at ALS, and Parrat Multilayer Recursion was used to fit thicknesses to the reflection data.[26,27]

The absorption part of the index of refraction will be extracted using equation 1:

$$T = \frac{I}{I_0} = e^{\frac{-4\pi\beta}{\lambda}r} \tag{1}$$

where T is the transmission, I is the intensity of the EUV beam through the iron sample, I_0 is the intensity of the EUV beam without iron, β is the absorption part of the index of refraction, λ is the wavelength of the

Downloaded From: https://www.spiedigitallibrary.org/conference-proceedings-of-spie on 09 Oct 2023
Terms of Use: https://www.spiedigitallibrary.org/terms-of-use

light, and r is the thickness of the material.[28] The measured data contains transmission through both iron and gold deposited on the photodiode. Thus the gold transmission is removed by dividing the measured intensity through the gold using the optical constants found on CXRO. We then compared the calculated β curve of the iron from the data taken at beamline 6.3.2 with the β values found at CXRO and the results are shown in Fig. 3B. The ALS data confirms that the binding energy of iron agrees with those reported on the CXRO website. The ALS data was used to more carefully calibrate the HHG spectrum. Additionally, we fitted the HHG data to the grating equation.

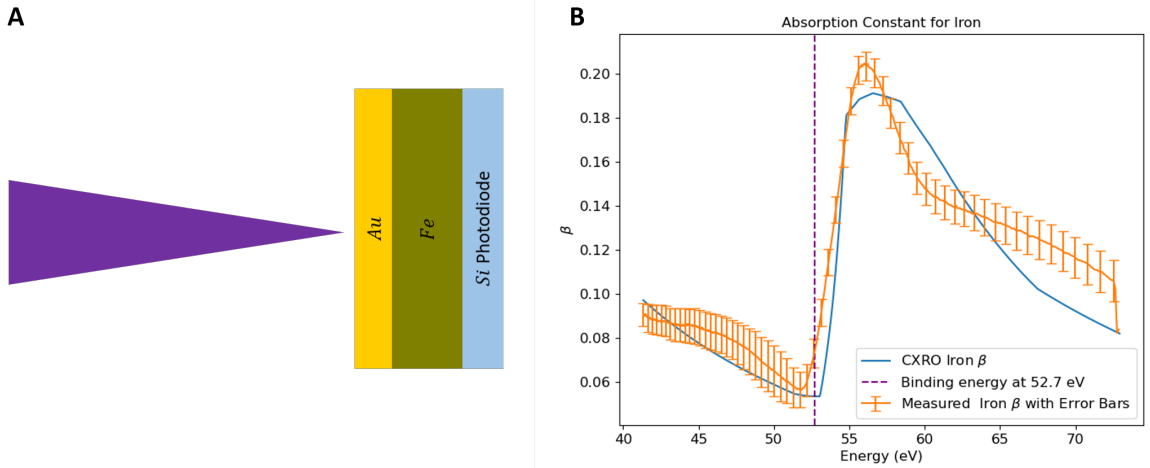


Figure 3. Synchrotron calibration at the iron $M_{2,3}$ edge in transmission geometry: (A) Schematic of iron deposited on silicon diode capped with a thin layer of gold for protection against oxidation. (B) Plots of β, the absorption part of the index of refraction as a function of energy extracted from the transmission measurements using a photodiode and the thicknesses from 2B. The orange curve is β which was calculated using equation 1 and the data taken from beamline 6.3.2 at ALS. The blue curve is the β values taken from CXRO. The purple dashed line indicates the location of the 52.7 eV resonance energy of iron.

To reconcile the ALS data with the HHG spectrum, we needed to consider more carefully how the harmonics were generated. The spectrum of our driving laser as been measured and is shown in Fig. 4A. Many of the wavelengths in this bandwidth could be used to drive the HHG process. We also have considered the effect of how the HHG spectrum will be affected by adjusting the chirp of the ultrafast pulse. Changing the chirp of the fundamental driving laser pulse can cause a red or blue shift (down or up in energy) to the HHG spectrum.[29,30] We optimized the HHG circular spectrum to obtain the brightest signal by adjusting the chirp using the the Ti:Sapphire compressor. We then measured both the linear and circular spectrum. Afterwards, we introduced additional chirp to the HHG linear spectrum. We recorded another linear HHG spectrum to observe the effects of chirp on the HHG process. The results are in Fig. 4B. The spectrum was blue shifted and its bandwidth broadened. This indicated that we may have introduced a negative chirp to the fundamental pulse which caused it to lengthen.[29,30] Fig. 4B depicts a blue shift by nearly a harmonic order in the HHG spectrum. This evidence suggests that we must be generating harmonics at a wavelength shorter than 800 nm.

We begin calibration of our HHG data by using a model to fit our separated harmonics. This fit was conducted using equation 2:

$$\begin{aligned}(y_i - y_0)^2 &= d_i^2 + d_0^2 - 2d_0 d_i \cos(\beta_i - \beta_0) \\ \beta_{i,0} &= \arcsin(m\lambda_{i,0}\sigma - \sin\alpha)\end{aligned} \tag{2}$$

Here, $y_{i,0}$ is the pixel location of each harmonic(i^{th}) and a known wavelength(0) on the detector (Andor ikon-L), $d_{i,0}$ is the distances wavelengths propagate from grating to detector, $\beta_{i,0}$ is the diffracted angles for each

Downloaded From: https://www.spiedigitallibrary.org/conference-proceedings-of-spie on 09 Oct 2023
Terms of Use: https://www.spiedigitallibrary.org/terms-of-use

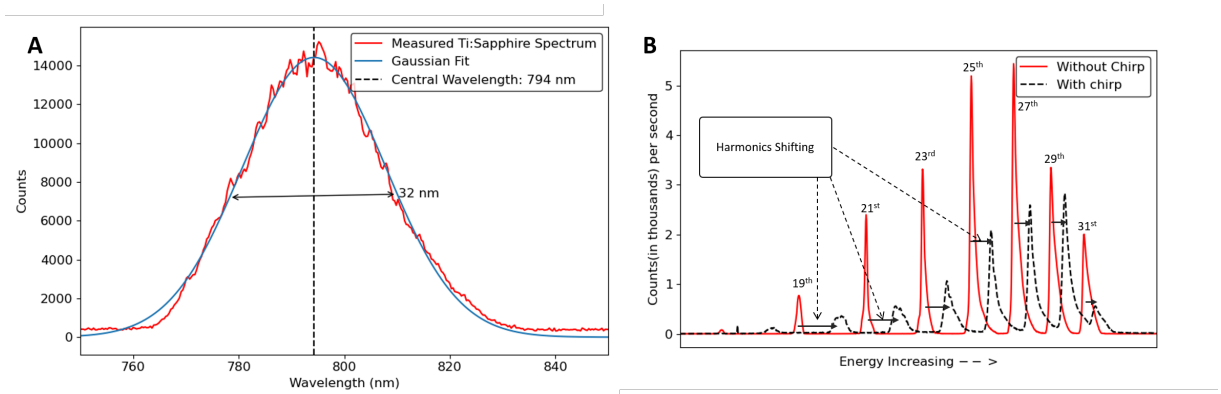


Figure 4. (A) Measured spectrum of the Ti:Sapphire laser with a Gaussian fit. The laser wavelength is centered at 794 nm with a bandwidth of 32 nm. (B) Plots of the HHG spectrum with the iron filter inserted. The solid red curve is obtained with the optimal chirp in the driving laser pulse. The dashed black curve is introducing more chirp into the driving laser pulse.

wavelength, $\lambda_{i,0}$ are the wavelengths, σ is the groove density of the grating (1200 grooves/mm), m is the diffraction order, and α is the angle of incidence on the diffraction grating. Equation 2 was derived using the reflective grating equation and the law of cosines.[28] Fig. 5A depicts the model of equation 2. The goodness of the fit was determined using the reduced chi-squared. The results for the fits of both the circularly and linearly polarized spectra are shown in Fig. 5B and 5C, respectively. The optimal wavelengths are 772 nm for circularly and 773 nm for linearly polarized spectra.

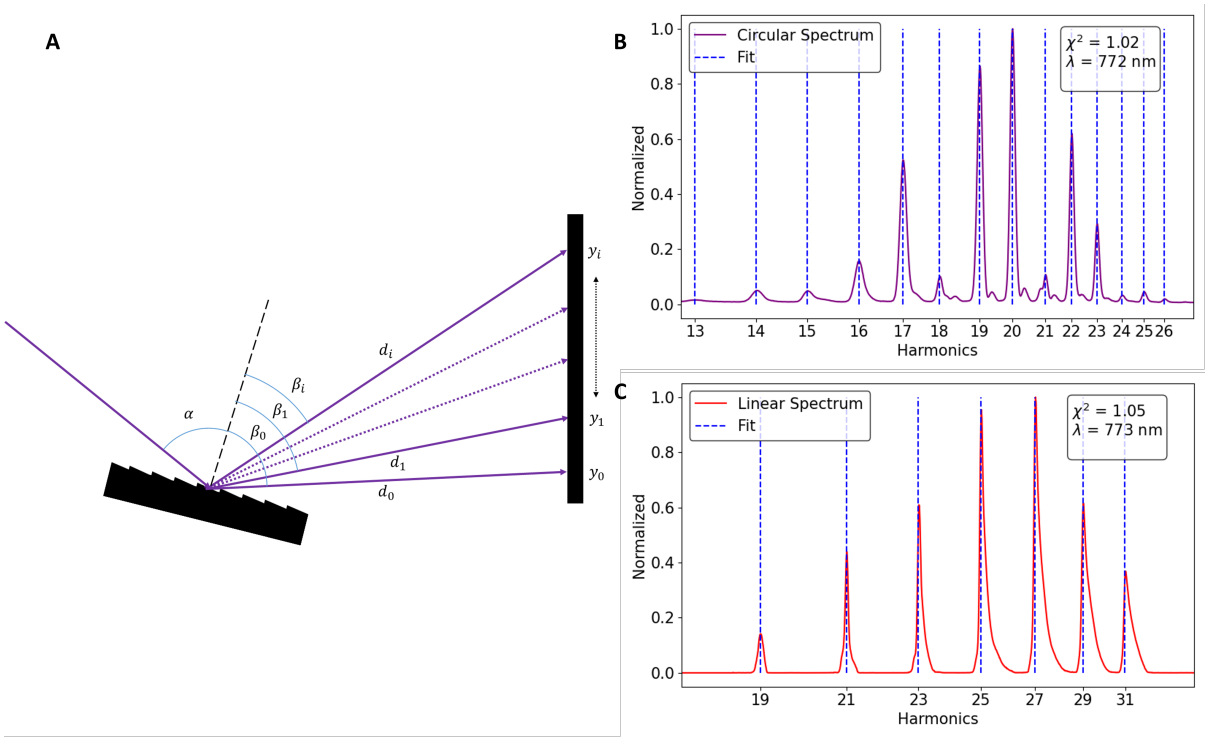


Figure 5. (A) Diagram of the EUV grating and setup used to calibrate the spectrum described in equation 2. (B) Model fitted peak locations for the circularly polarized spectrum. The blue dashed lines represent the the fitted locations of the harmonics. The reduced chi-squared is 1.02 with the optimized fundamental wavelength parameter at 772 nm. (C) Model fitted peak locations for the linearly polarized spectrum. The reduced chi-squared is 1.05 with optimized fundamental wavelength parameter at 773 nm.

Downloaded From: https://www.spiedigitallibrary.org/conference-proceedings-of-spie on 09 Oct 2023
Terms of Use: https://www.spiedigitallibrary.org/terms-of-use

Using the wavelengths from the fits and the β data taken from ALS, we created a transmission curve for a 100 nm iron filter and compared it with the transmission curve obtained from the HHG data. The HHG transmission curve was generated by taking two spectra of the HHG, one with 100 nm iron filter inserted and the other with a 100 nm aluminum filter inserted, and dividing the spectra by each other. The results are shown in Fig. 6A. The horizontal axis of the red curves (HHG) were fitted using known wavelengths and their pixel locations on the Andor ikon-L control software. The harmonics in this figure suggest the driving wavelength is 773 ± 3 nm. This would explain the discrepancy we saw in Fig. 1. The 33$^{\text{rd}}$ harmonic would have a photon energy of 52.9 eV which will be greatly absorbed by the iron filters. We have now successfully calibrated the HHG spectrum using the results obtained from ALS and it is shown in Fig. 6B.

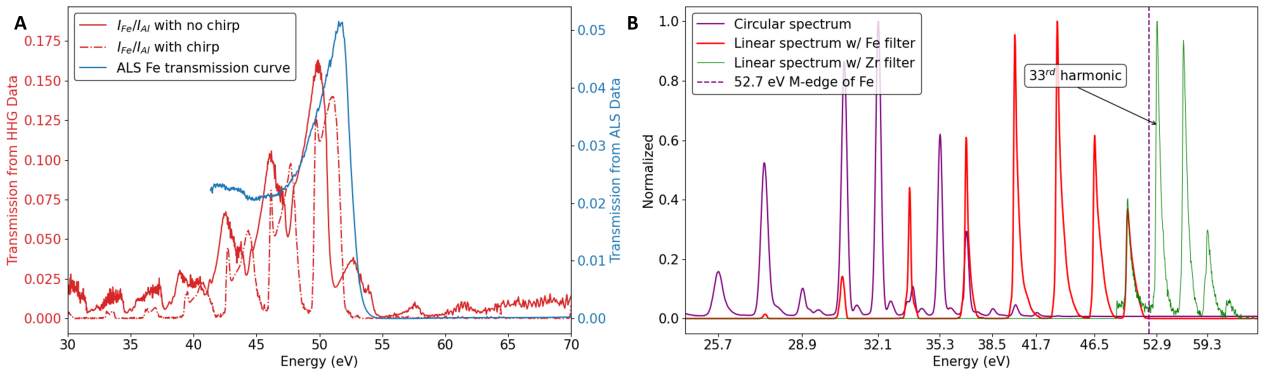


Figure 6. (A) Plots of the calculated ALS and HHG transmission. (B) Calibrated HHG spectra using the results from the ALS data. Energies of several harmonics are indicate on x-axis. The 33$^{\text{rd}}$ harmonic would have an energy of 52.9 eV which will have very low transmission. Vertical dashed purple line indicates location of 52.7 eV M-absorption edge of iron.

3. CONCLUSION

HHG is a promising source for probing magnetism. To obtain magnetic contrast, these sources require careful calibration techniques as described in this paper. Metal filters are effective at identifying harmonics in the HHG spectrum. We have confirmed that $M_{2,3}$ edge of iron is at 52.7 eV at ALS and used the results to calibrate the HHG spectrum of our EUV source at Brigham Young University. The calibration revealed that we were driving the harmonics with 773 ± 3 nm wavelengths. When calibrating HHG systems, it is important to consider that the driving wavelength is not necessarily the central wavelength of the driving laser beam. Several wavelengths can drive the HHG process since the driving laser beam has a broad bandwidth and due to the extreme nonlinear nature of HHG. It is important to note that adjusting the chirp of the fundamental pulse could cause the HHG spectrum to shift in energy. This can be used to tune the HHG spectrum to the resonant energies of magnetic materials. These accurate calibrations for HHG sources are required to effectively probe magnetism in materials.

ACKNOWLEDGMENTS

This work has been supported by the Department of Physics and Astronomy and the College of Physical and Mathematical Science at Brigham Young University. This research used resources of the Advanced Light Source, which is a DOE Office of Science User Facility under contract no. DE-AC02-05CH11231.

REFERENCES

[1] Corkum, P. B., "Plasma perspective on strong field multiphoton ionization," *Physical Review Letters* **71**(13), 1994–1997 (1993).

[2] Buckway, T., *Tabletop Extreme-Ultraviolet Source Using High Harmonic Generation for Polarization Sensitive Imaging*, PhD thesis, Brigham Young Unversity, Provo (2022).

[3] Kapteyn, H. C., Murnane, M. M., and Christov, I. P., "Extreme Nonlinear Optics: Coherent X rays from Lasers," *Physics Today* **58**(3), 39–46 (2005).

Downloaded From: https://www.spiedigitallibrary.org/conference-proceedings-of-spie on 09 Oct 2023
Terms of Use: https://www.spiedigitallibrary.org/terms-of-use

[4] Lytle, A. L., *Phase Matching and Coherence of High-Order Harmonic Generation in Hollow Waveguides*, PhD thesis, University of Colorado (2001).

[5] Popmintchev, T., *Tunable ultrafast coherent light in the soft and hard X-ray regions of the spectrum: Phase matching of extreme high-order harmonic generation*, PhD thesis, University of Colorado at Boulder (2010).

[6] Sandberg, R. L., Song, C., Wachulak, P. W., Raymondson, D. A., Paul, A., Amirbekian, B., Sakdinawat, A. E., Lee, E., La-O-Vorakiat, C., Marconi, M. C., Menoni, C. S., Murnane, M. M., Rocca, J. J., Kapteyn, H. C., and Miao, J., "70 nm Lensless Diffractive Microscopy using Tabletop Soft X-ray Sources," in [*Conference on Lasers and Electro-Optics/Quantum Electronics and Laser Science Conference and Photonic Applications Systems Technologies*], CMCC5, Optical Society of America (2008).

[7] Seaberg, M. D., Zhang, B., Gardner, D. F., Shanblatt, E. R., Murnane, M. M., Kapteyn, H. C., and Adams, D. E., "Tabletop nanometer extreme ultraviolet imaging in an extended reflection mode using coherent Fresnel ptychography," *Optica* **1**(1), 39–44 (2014).

[8] Fan, T., Grychtol, P., Knut, R., Hernández-García, C., Hickstein, D. D., Zusin, D., Gentry, C., Dollar, F. J., Mancuso, C. A., Hogle, C. W., Kfir, O., Legut, D., Carva, K., Ellis, J. L., Dorney, K. M., Chen, C., Shpyrko, O. G., Fullerton, E. E., Cohen, O., Oppeneer, P. M., Milošević, D. B., Becker, A., Jaroń-Becker, A. A., Popmintchev, T., Murnane, M. M., and Kapteyn, H. C., "Bright circularly polarized soft X-ray high harmonics for X-ray magnetic circular dichroism," *Proceedings of the National Academy of Sciences* **112**(46), 14206–14211 (2015).

[9] Vura-Weis, J., Jiang, C. M., Liu, C., Gao, H., Lucas, J. M., De Groot, F. M., Yang, P., Alivisatos, A. P., and Leone, S. R., "Femtosecond M2,3-edge spectroscopy of transition-metal oxides: Photoinduced oxidation state change in α-Fe2O3," *Journal of Physical Chemistry Letters* **4**(21), 3667–3671 (2013).

[10] Kfir, O., Zayko, S., Nolte, C., Sivis, M., Möller, M., Hebler, B., Arekapudi, S. S. P. K., Steil, D., Schäfer, S., Albrecht, M., Cohen, O., Mathias, S., and Ropers, C., "Nanoscale magnetic imaging using circularly polarized high-harmonic radiation," *Science Advances* **3**(12), eaao4641 (2017).

[11] Alves, C., *Studying ultrafast magnetization dynamics through Faraday effect and using linearly polarized high order harmonics*, PhD thesis, Sorbonne University (2018).

[12] Stohr, J. and Siegmann, H., [*Interactions of Polarized Photons with Matter*], 351–429, Springer Berlin Heidelberg, Berlin, Heidelberg (2006).

[13] Cai, Y. P., Chesnel, K., Trevino, M., Westover, A., Harrison, R. G., Hancock, J. M., Turley, S., Scherz, A., Reid, A., Wu, B., Graves, C., Wang, T., Liu, T., and Dürr, H., "Orbital and spin moments of 5 to 11 nm Fe3O4 nanoparticles measured via x-ray magnetic circular dichroism," *Journal of Applied Physics* **115**(17), 17B537 (2014).

[14] Chesnel, K., Griner, D., Smith, D., Cai, Y., Trevino, M., Newbold, B., Wang, T., Liu, T., Jal, E., Reid, A. H., and Harrison, R. G., "Unraveling Nanoscale Magnetic Ordering in Fe3O4 Nanoparticle Assemblies via X-rays," *Magnetochemistry* **4**(4) (2018).

[15] Hennes, M., Rösner, B., Chardonnet, V., Chiuzbaian, G. S., Delaunay, R., Döring, F., Guzenko, V. A., Hehn, M., Jarrier, R., Kleibert, A., Lebugle, M., Lüning, J., Malinowski, G., Merhe, A., Naumenko, D., Nikolov, I. P., Lopez-Quintas, I., Pedersoli, E., Savchenko, T., Watts, B., Zangrando, M., David, C., Capotondi, F., Vodungbo, B., and Jal, E., "Time-Resolved XUV Absorption Spectroscopy and Magnetic Circular Dichroism at the Ni M2,3-Edges," *Applied Sciences* **11**(1), 325 (2020).

[16] Kfir, O., Bordo, E., Ilan Haham, G., Lahav, O., Fleischer, A., and Cohen, O., "In-line production of a bi-circular field for generation of helically polarized high-order harmonics," *Applied Physics Letters* **108**(21), 211106 (2016).

[17] Kfir, O., Grychtol, P., Turgut, E., Knut, R., Zusin, D., Popmintchev, D., Popmintchev, T., Nembach, H., Shaw, J. M., Fleischer, A., Kapteyn, H., Murnane, M., and Cohen, O., "Generation of bright phase-matched circularly-polarized extreme ultraviolet high harmonics," *Nature Photonics* **9**(2), 99–105 (2015).

[18] Fleischer, A., Kfir, O., Diskin, T., Sidorenko, P., and Cohen, O., "Spin angular momentum and tunable polarization in high-harmonic generation," *Nature Photonics* **8**(7), 543–549 (2014).

[19] Long, S., Becker, W., and McIver, J. K., "Model calculations of polarization-dependent two-color high-harmonic generation," *Phys. Rev. A* **52**, 2262–2278 (sep 1995).

Downloaded From: https://www.spiedigitallibrary.org/conference-proceedings-of-spie on 09 Oct 2023
Terms of Use: https://www.spiedigitallibrary.org/terms-of-use

[20] Constant, E., Garzella, D., Breger, P., Mével, E., Dorrer, C., Le Blanc, C., Salin, F., and Agostini, P., "Optimizing High Harmonic Generation in Absorbing Gases: Model and Experiment," *Phys. Rev. Lett.* **82**(8), 1668–1671 (1999).

[21] Alon, O. E., Averbukh, V., and Moiseyev, N., "Selection Rules for the High Harmonic Generation Spectra," *Phys. Rev. Lett.* **80**(17), 3743–3746 (1998).

[22] Armstrong, J. A., Bloembergen, N., Ducuing, J., and Pershan, P. S., "Interactions between Light Waves in a Nonlinear Dielectric," *Physical Review* **127**(6), 1918 (1962).

[23] Eric Gullikson, "X-Ray Interactions with Matter," (2022).

[24] Fuggle, J. C. and Mårtensson, N., "Core-level binding energies in metals," *Journal of Electron Spectroscopy and Related Phenomena* **21**(3), 275–281 (1980).

[25] Lebugle, A., Axelsson, U., Nyholm, R., and Mprtensson, N., "Experimental L and M Core Level Binding Energies for the Metals 22Ti to 30Zn," *Physica Scripta* **23**(5A), 825 (1981).

[26] Muhlestein, J. B., Smith, B. D., Miles, M., Thomas, S. M., Willey, A., Allred, D. D., and Turley, R. S., "Y2O3 optical constants between 5 nm and 50 nm," *Opt. Express* **27**(3), 3324–3336 (2019).

[27] Parratt, L. G., "Surface studies of solids by total reflection of x-rays," *Phys. Rev.* **95**, 359–369 (1954).

[28] Attwood, D. and Sakdinawat, A., [*X-Rays and Extreme Ultraviolet Radiation: Principles and Applications*], Cambridge University Press, 2 ed. (2017).

[29] Zhou, J., Peatross, J., Murnane, M. M., Kapteyn, H. C., and Christov, I. P., "Enhanced High-Harmonic Generation Using 25 fs Laser Pulses," *Phys. Rev. Lett.* **76**(5), 752–755 (1996).

[30] Lavocat-Dubuis, X., Vidal, F., Matte, J. P., Popovici, C., Ozaki, T., and Kieffer, J. C., "Effects of chirp and pulse shape on high harmonic generation and absorption in overdense plasmas," *Laser and Particle Beams* **29**(1), 95–104 (2011).

Downloaded From: https://www.spiedigitallibrary.org/conference-proceedings-of-spie on 09 Oct 2023
Terms of Use: https://www.spiedigitallibrary.org/terms-of-use